DOI 10.1007/s11041-023-00963-6
*Metal Science and Heat Treatment*, Vol. 65, Nos. 7 – 8, November, 2023 (Russian Original Nos. 7 – 8, July – August, 2023)

# STRUCTURAL STEELS

UDC 669.018.298:620.186/.187:620.172.2/178.7

# EVOLUTION OF GRADIENT STRUCTURE UNDER HEAT TREATMENT OF METASTABLE AUSTENITIC STAINLESS STEEL SUBJECTED TO COLD RADIAL FORGING

**D. O. Panov,[1] E. A. Kudryavtsev,[1] A. V. Naumov,[1] A. S. Pertsev,[1] Yu. N. Simonov,[1] and G. A. Salishchev[1]**

Translated from *Metallovedenie i Termicheskaya Obrabotka Metallov*, No. 8, pp. 58 – 66, August, 2023.

*Original article submitted December 6, 2022.*

The effect of heat treatment on the structure and mechanical properties of a metastable austenitic steel subjected initially to cold radial forging is studied. The evolution of the phase composition, of the structure and of the texture is investigated. The strength, the ductility and the impact toughness are determined as a function of the annealing temperature. It is shown that the cold radial forging yields a gradient distribution of strain martensite over cross section. Subsequent annealing at 500°C causes precipitation hardening of the strain martensite due to precipitation of nanocarbides. In addition to the considerable hardening ($\sigma_r > 1500$ MPa) this is accompanied by formation of a high-toughness state ($KCT > 1.4$ MJ/m$^2$). Medium-temperature (650°C) annealing produces a structure represented by clusters of fine grains of austenite and martensite with orientations $\langle 111 \rangle_A \parallel$ PA and $\langle 101 \rangle_M \parallel$ PA parallel to the bar axis (PA) and coarse austenite grains with orientation $\langle 001 \rangle_A \parallel$ PA. This provides a combination of high strength ($\sigma_r > 1100$ MPa), ductility ($\delta > 20\%$) and impact toughness ($KCT \sim 1.3$ MJ/m$^2$).

***Key words:*** metastable austenitic stainless steel, radial forging, gradient structure, strength, ductility, impact toughness.

## INTRODUCTION

Metastable austenitic stainless steels possess high corrosion resistance, ductility and adaptability to manufacture [1, 2]. At the same time, their low yield strength limits their application, for example, in highly loaded components of constructions and machine parts. Elevation of the strength characteristics by refinement of structure is commonly accompanied by a loss in ductility [3 – 5] and impact toughness [16], which makes it necessary to search for a compromise between the hardening and the ductility loss.

It is known that formation of gradient structures makes it possible to obtain multifunctional properties [7 – 11]. A gradient (graded) structure is usually understood as gradual variation of the phase composition, of the grain size or of the density of crystal structure defects from the surface to the core of the billet. When such materials are tensed, plastic deformation develops primarily over the soft core, while the stresses concentrate in the hardened surface layers [12]. For example, copper with a gradient structure possess an elevated strength and a ductility comparable to that of coarse-grained copper [7]. Similar effects have been observed in a metastable austenitic stainless steel [11], which had an ultrafine-grained austenitic structure on the surface and a coarse-grained structure in the core. In addition, this may be accompanied by elevation of the low-cycle and high-cycle fatigue strength [10] and by improvement of the corrosion resistance [11].

It should be noted that the relatively high mechanical properties of materials with gradient structure have been ob-

[1] Belgorod State National Research University, Belgorod, Russia (e-mail: dimmak-panov@mail.ru).
[2] Perm State Research Technological Institute, Perm, Russia.
[3] Perm National Research Polytechnic University, Perm, Russia.

tained in most cases for relatively small specimens and a depth of the structural gradient of at most 200 μm. The mechanical properties of materials with gradient structure of a larger scale require special consideration. It has been shown earlier that cold radial forging can give a larger-scale gradient structure in a metastable austenitic stainless steel 08Kh18N10T (of type AISI 321) [13]. However, systematic studies of the evolution of such structures and of mechanical properties under heat treatment have not been performed.

The aim of the present work was to study the effect of heat treatment on the evolution of the gradient structure and mechanical properties of metastable austenitic stainless steel 08Kh18N10T subjected preliminarily to cold radial forging.

## METHODS OF STUDY

We studied steel 08Kh18N10T of the following chemical composition (in wt.%): 0.07 C, 18.75 Cr, 9.20 Ni, 1.12 Mn, 0.59 Ti, 0.39 Si, 0.019 P, 0.005 S. Bars with diameter 33 mm were hot-forged at 900 – 1200°C with air cooling. Subsequent austenitization was conducted at 1050°C for 1 h with water cooling, which provided a homogeneous austenitic structure with a mean grain size of $10 \pm 1$ μm. The structure also contained less than 2% δ-ferrite [6]. Then the bars were deformed in an SXP-16 radial forging machine at room temperature. The deformation source was cooled with water continuously. The radial forging was conducted in five passes, i.e., (*1*) from ∅33 to ∅29 mm, (*2*) from ∅29 to ∅25 mm, (*3*) from ∅25 to ∅20 mm, (*4*) from ∅20 to ∅14 mm, and (*5*) from ∅14 to ∅11.3 mm. The total reduction ε was about 90%. The post-deformation annealing was conducted at 400, 500, 550, 600, 650, 700, 800 and 900°C with a hold for 2 h and air cooling.

The fine structure was studied on foils with the help of a JEOL JEM-2100 transmission electron microscope at an accelerating voltage of 200 kV. The EBSD analysis was made using a FEI Nova NanoSEM 450 scanning electron microscope equipped with a EDAX Hikari EBSD camera. The data obtained were analyzed using the TSL OIM Analysis software.

The foils were fabricated from billets with a thickness of 0.3 mm cut over cross section of the bars with an electroerosion mill. The foils were thinned uniformly on both sides against emery papers with different grains sizes. Then they were subjected to electrolytic thinning to form a hole using a TenuPol-5 device in an electrolyte composed of 5% perchloric acid, 35% butanol and 60% ethanol.

The distribution of the ferromagnetic phase (α′-martensite and δ-ferrite) was determined over the diameter of the bars by the eddy-current method using a FERRITSCOPE FMP30 device calibrated preliminarily using reference samples. We made three measurements per point and processed the results statistically.

The Vickers hardness was measured over two mutually perpendicular diameters using a Wolpert 402MCD semiautomatic hardness tester at a load of 200 g with 15-sec exposure. The diamond pyramid had an angle of 136° at the vertex. The results of the measurements at equivalent points over two tracks were averaged.

The tests for uniaxial tension were carried out in an INSTRON-SATEC 300 LX universal hydraulic system for static tests. The strength ($\sigma_r$, $\sigma_{0.2}$) and ductility (δ, ψ) characteristics were determined for five-fold cylindrical samples of type III No. 7 according to the GOST 1497–84 Standard.

The tests for dynamic three-point bending with determination of the *KCT* impact toughness were conducted at room temperature using a PSWO-30 pendulum impact tester for samples of type 17 according to GOST 9454–78.

## RESULTS AND DISCUSSION

***Evolution of structure under heat treatment.*** Prior to the cold radial forging (CRF), the content of δ-ferrite in the structure of steel 08Kh18N10T was uniform over cross section and did not exceed 2% [6]. Right after the CRF, we detected a well manifested graded content of α′-martensite and δ-ferrite from the center to the edge of the billet (Fig. 1*a*). The center contained $38.9 \pm 1\%$ (α′ + δ)-phase; the edge contained $67.8 \pm 0.9\%$. It is obvious that this distribution may be associated with nonuniform development of the strain-induced martensitic transformation during the CRF, the degree of which is determined by the accumulated plastic strain in every region of the bar [14]. On the surface, where the deformation is more intense, the degree of the $\gamma \rightarrow \alpha'$ transformation is much higher than in the center.

After the annealing at 500°C, the content of the α-phase decreases somewhat over the whole of the cross section of the bar (Fig. 1*a*). By the data of [15], reverse martensitic $\alpha' \rightarrow \gamma$ transformation starts under the conditions of continuous heating at 530°C. By the data of the authors of [15], the used method of analysis of dilatometric results gives ≥ 1.5% fresh martensite under the $\alpha' \rightarrow \gamma$ transformation. However, under continuous heating, the $\alpha' \rightarrow \gamma$ transformation at 500°C has not been detected by the dilatometric analysis most probably due to the low development of the $\alpha' \rightarrow \gamma$ transformation (less than about 1.5%). It is obvious that the 2-h hold at 500°C has promoted the development of the $\alpha' \rightarrow \gamma$ transformation in an amount sufficient for detection by the eddy-current method.

Annealing at 550 – 600°C promotes development of the $\alpha' \rightarrow \gamma$ transformation more than at 500°C and hence reduces the content of the α-phase. The gradient of the phase composition over the cross section is preserved (Fig. 1*a*) and disappears almost fully only after annealing at 650°C.

The gradient of the content of α-phase after the CRF does not cause an obvious hardness gradient (Fig. 1*b*), because the hardness values of the mechanically hardened austenite and of the strain martensite in the structure of steel 08Kh18N10T are close [16]. However, there is some nonuni-

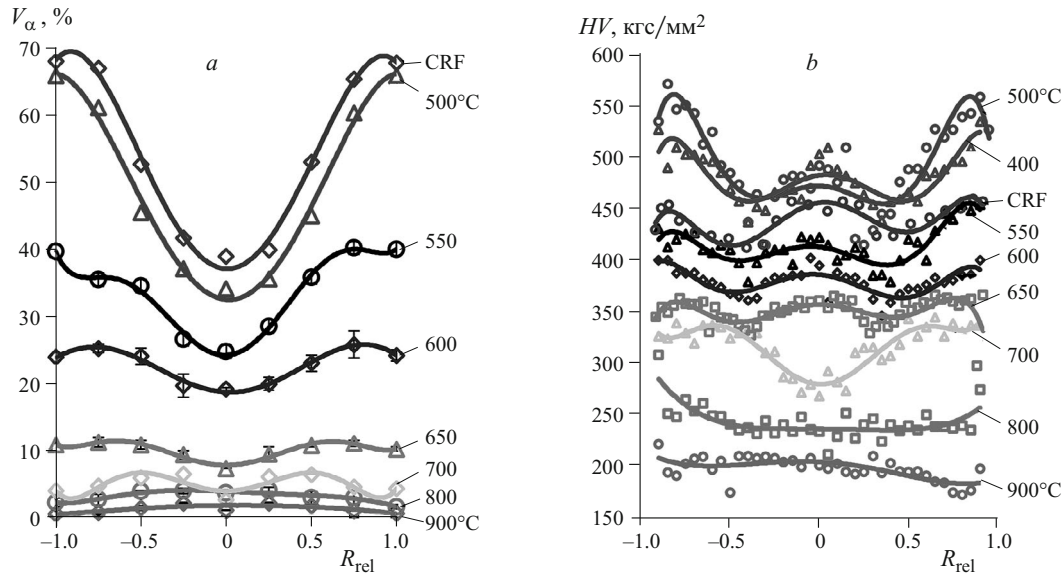


**Fig. 1.** Distribution of the α-phase $V_\alpha$ (*a*) and of the hardness (*b*) over the diameter of a bar from steel 08Kh18N10T after annealing at various temperatures (given at the curves): $R_{rel}$) distance from the center in fractions of the radius.

formity in the hardness distribution over the cross section after the CRF with degree 90%.

The highest hardness level is detected in the center and in the surface layers of the bar and is the lowest at half-radius. This effect seems to be explainable by the impact of residual stresses. For example, in accordance with the data of [17], the highest tensile stresses occur after the CRF in the center of the bar, while the surface regions are characterized by an elevated level of compressive stresses. At the middle of the radius the residual stresses are zero, which finds manifestation in the minimum hardness of this region (Fig. 1*b*).

After the annealing at 400 and 500°C, the general level of the hardness of the steel becomes much higher than after the CRF (Fig. 1*b*). The hardness of the surface layers increases the most. In its turn, the annealing at 550 – 700°C causes lowering of the general hardness level but does not remove the nonuniformity of its distribution (Fig. 1*b*). The annealing at 800 and 900°C results in uniformity of the hardness distribution over cross section and renders the hardness level close to the hardness of the initially undeformed steel 08Kh18N10T [6].

The studies of the microstructure show that cold radial forging of steel 08Kh18N10T produces a chiefly lamellar austenitic-martensitic structure in the center of the cross section (Fig. 2). At the same time, the near-surface layer has a chiefly globular martensitic structure (Fig. 2*b*). The width of the lamellas in the center and the diameter of the globules near the surface of the bar are close (170 – 180 nm). In the longitudinal section, the center and the surface have a finer structure (Fig. 2*c* and *d*).

Subsequent annealing at 500°C is accompanied by formation of fine recrystallization nuclei (with diameter $d \sim 100$ nm) (Fig. 3*a* and *b*). This results in some refinement of the structure from $170 \pm 10$ to $110 \pm 10$ nm in the center and from $180 \pm 15$ to $170 \pm 10$ nm at the surface of the bar. The crystals of strain martensite acquire $M_{23}C_6$-type nanocarbides $6 \pm 1$ nm in size inside the grains and $12 \pm 2$ nm in size over the boundaries (Fig. 3*c*). It should be noted that the sharp increase of the hardness after the annealing at 400 and 500°C (Fig. 1*b*) seems to be a result of precipitation hardening of α′-martensite [18]. For example, after the annealing at 500°C the nanocarbide hardening amounts to 120 MPa in the center and to 240 MPa at the surface of the bar [19]. Such evolution of the hardness is connected with the double difference in the contents of strain martensite (Fig. 1*a*).

After the annealing at 650°C the center of the bar bears austenite regions with a lath substructure (Fig. 4*a*) due to the shear reverse $\alpha \rightarrow \gamma$ transformation [15, 20]. In addition, the coarse austenite grains in the structure are accompanied by conglomerates of fine globular austenite and martensite grains (Fig. 4*b*). Such grains seem to appear as a result of both reverse diffusion $\alpha \rightarrow \gamma$ transformation and of recrystallization of the mechanically hardened austenite [15, 20]. At the surface of the bar, we observe chiefly fine equiaxed austenite and martensite grains (Fig. 4*c*). After the annealing at 800°C the center and the surface of the bar acquire a structure of polyhedral austenite (Fig. 4*d* and *e*). It should be noted that the increase of the annealing temperature is also accompanied by coagulation of carbides.

The results of the EBSD analysis are presented in Figs. 5 and 6. After the annealing at 650°C the center of the bar acquires a well manifested two-component austenitic texture $\langle 001 \rangle_A \parallel$ PA and $\langle 111 \rangle_A \parallel$ PA (here PA is the texture parallel to the axis of the bar) (Fig. 5*a*). The grains with orientation

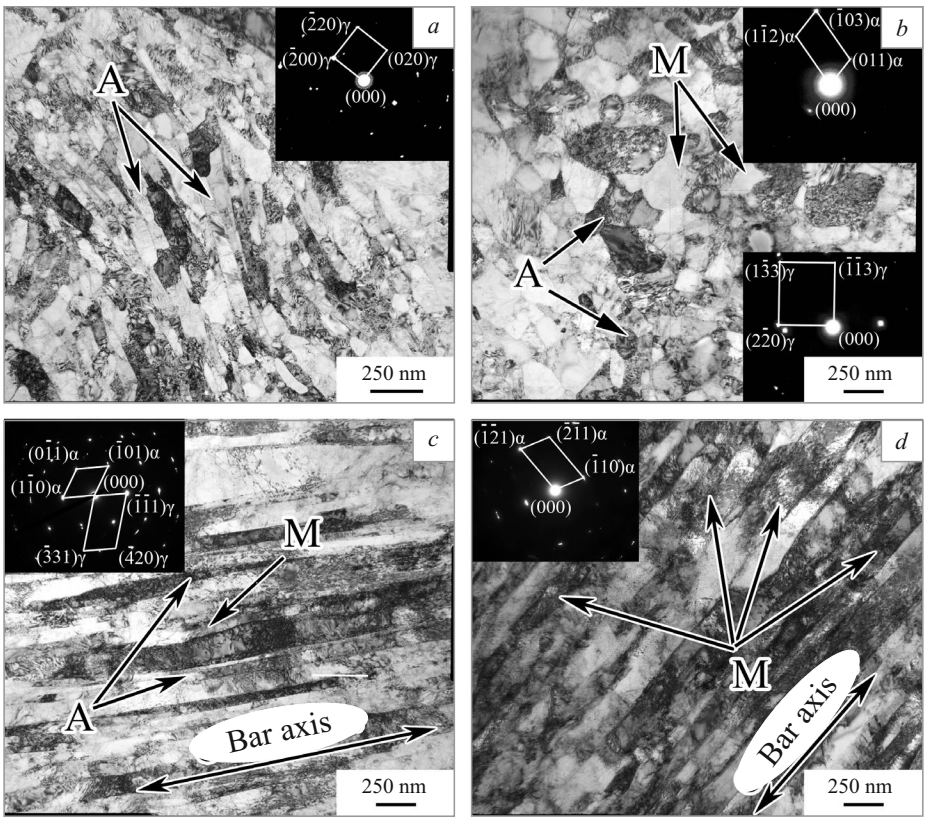


**Fig. 2.** Structures of austenite (A, γ) and martensite (M, α) and microdiffraction from them in the center (*a*, *c*) and in the surface layer (*b*, *d*) of a bar from steel 08Kh18N10T after CRF: *a*, *b*) cross section; *c*, *d*) longitudinal section.

$\langle 001\rangle_A \parallel$ PA are relatively coarse. On the contrary, the austenite grains with orientation $\langle 111\rangle_A \parallel$ PA are fine due to the action of the pinning effect from the clusters of martensite grains [20] in such regions (Fig. 6*a*). The martensite crystals produced by the CRF have orientation $\langle 101\rangle_M \parallel$ PA [21]. Our data show that the martensite and the austenite obey the Kurdyumov–Sachs orientation relationship. At the surface of the bar we observe a dominantly single-component texture $\langle 111\rangle_A \parallel$ PA (Fig. 5*d*) and a poorly manifested texture $\langle 001\rangle_A \parallel$ PA. In this case, the grains with orientation $\langle 111\rangle_A \parallel$ PA are also quite fine and are distributed uniformly in the subsurface layers, which is explainable by the presence of fine grains of strain martensite (Figs. 5*d* and 6*b*).

Annealing at 700°C is accompanied by substantial growth of the austenite grains in the center (Fig. 5*b*). At the surface, we still observe a fine-grained austenitic structure (Fig. 5*e*). Annealing at 800°C causes considerable coarsening of the grain structure both in the center (Fig. 5*b*) and at the surface (Fig. 5*f*). The proportion of the grains with orientation $\langle 111\rangle_A \parallel$ PA in the center of the bar decreases from about 35% to about 20% at a virtually invariable content (about 37 – 41%) of grains with orientation $\langle 001\rangle_A \parallel$ PA (see

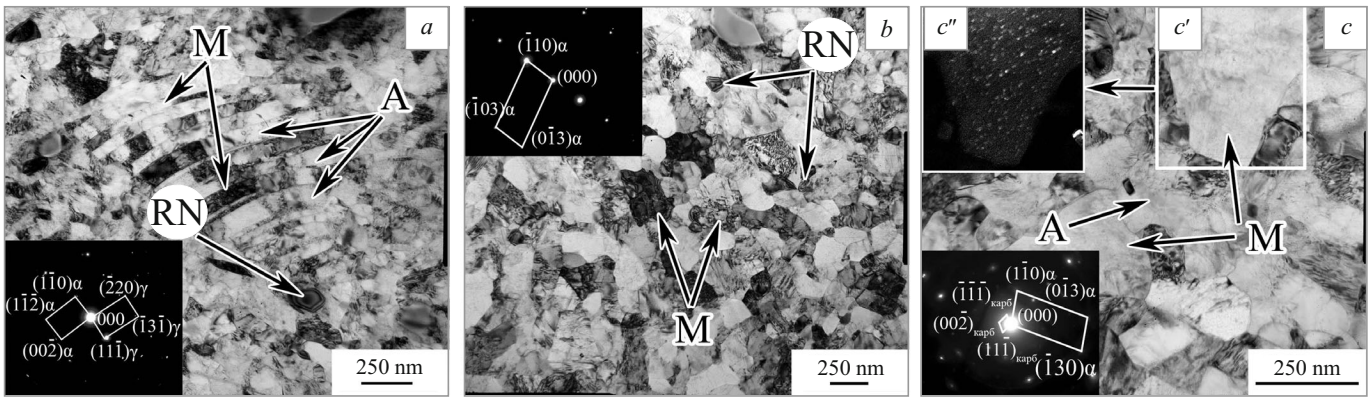


**Fig. 3.** Structure and microdiffraction from the center (*a*) and from the surface layer (*b*, *c*) in cross section of a bar from steel 08Kh18N10T after CRF and annealing at 500°C: *c*′ and *c*″) martensite region and its dark-background image in reflection (11-1) of $M_{23}C_6$ carbide, respectively.

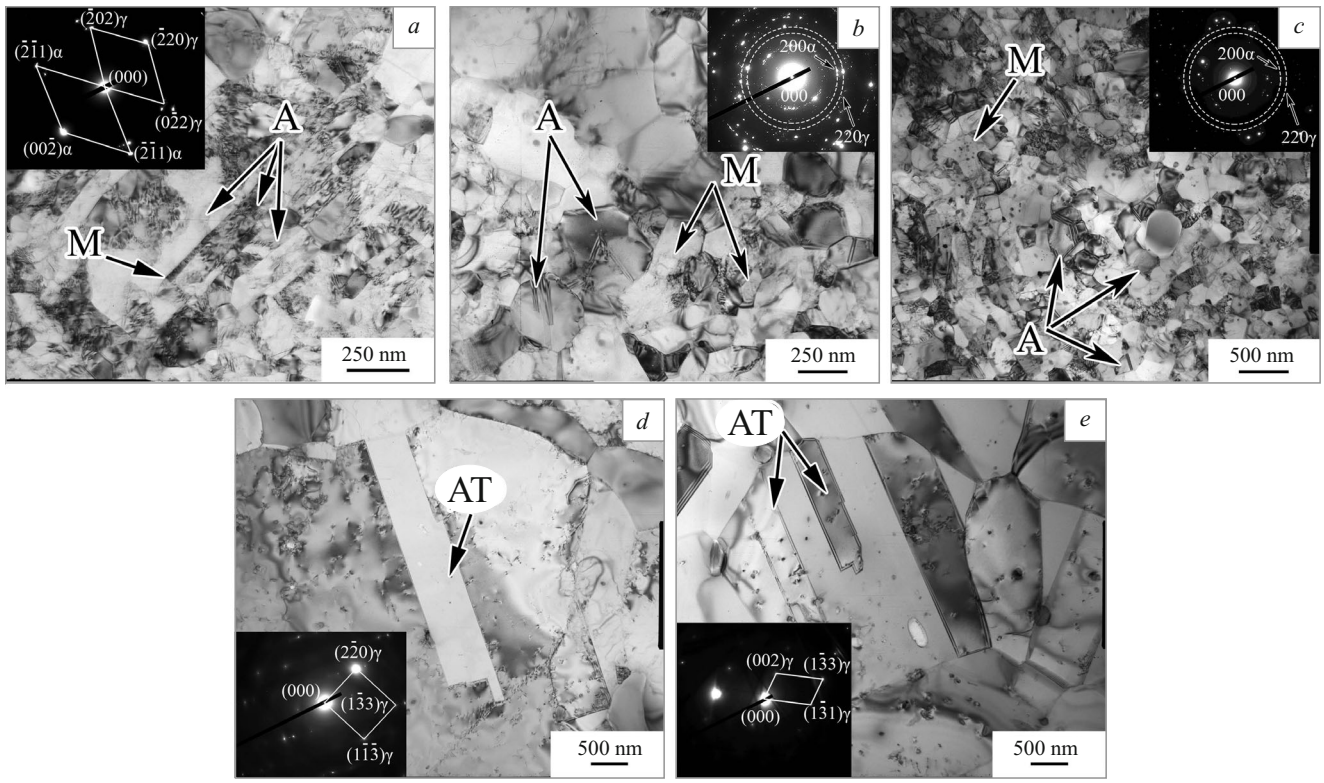


**Fig. 4.** Structure and microdiffraction from the center (*a*, *b*, *d*) and from the surface layer (*c*, *e*) in cross section of a bar from steel 08Kh18N10T after CRF and annealing at 650°C (*a* – *c*) and 800°C (*d*, *e*).

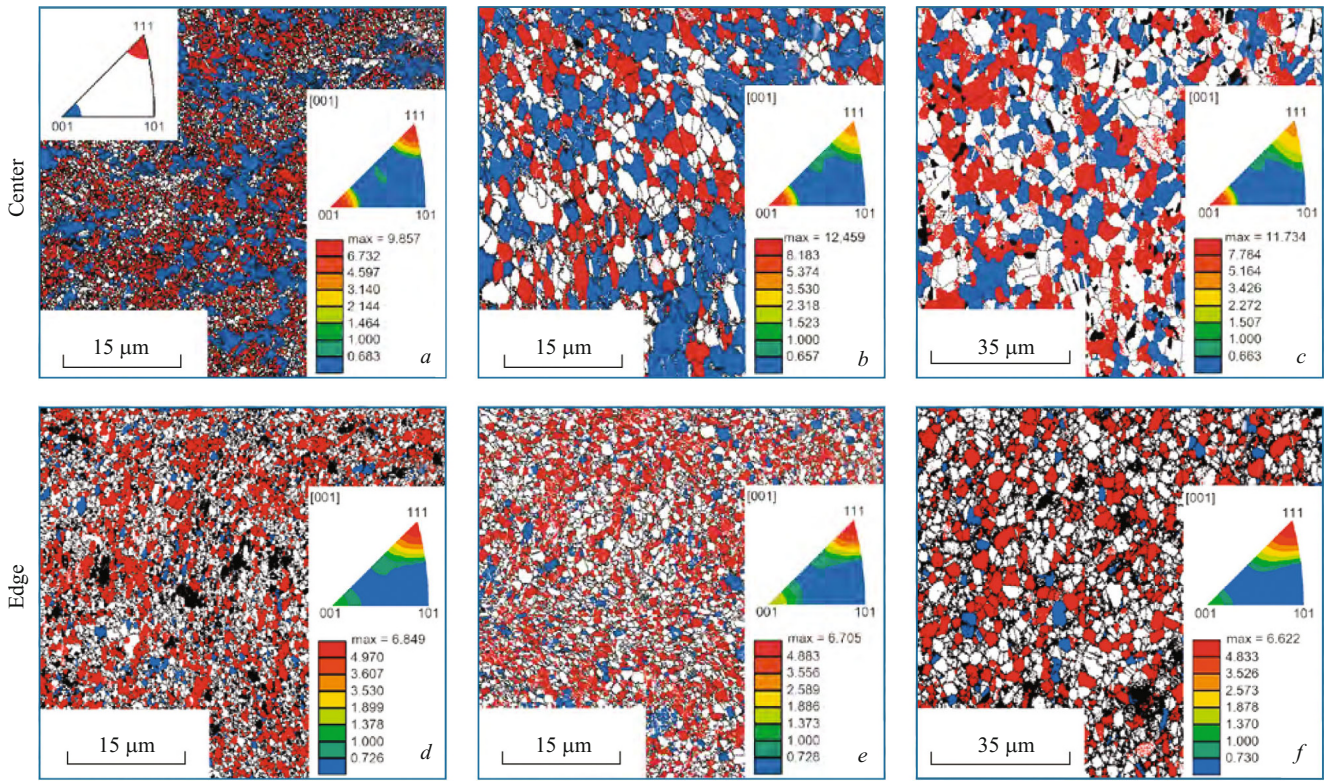


**Fig. 5.** Texture maps of austenitic structure in the center (*a* – *c*) and in the surface layer (*d* – *f*) of a bar from steel 08Kh18N10T (cross section) after cold radial forging and annealing at different temperatures: *a*, *d*) 650°C; *b*, *e*) 700°C; *c*, *f*) 800°C.

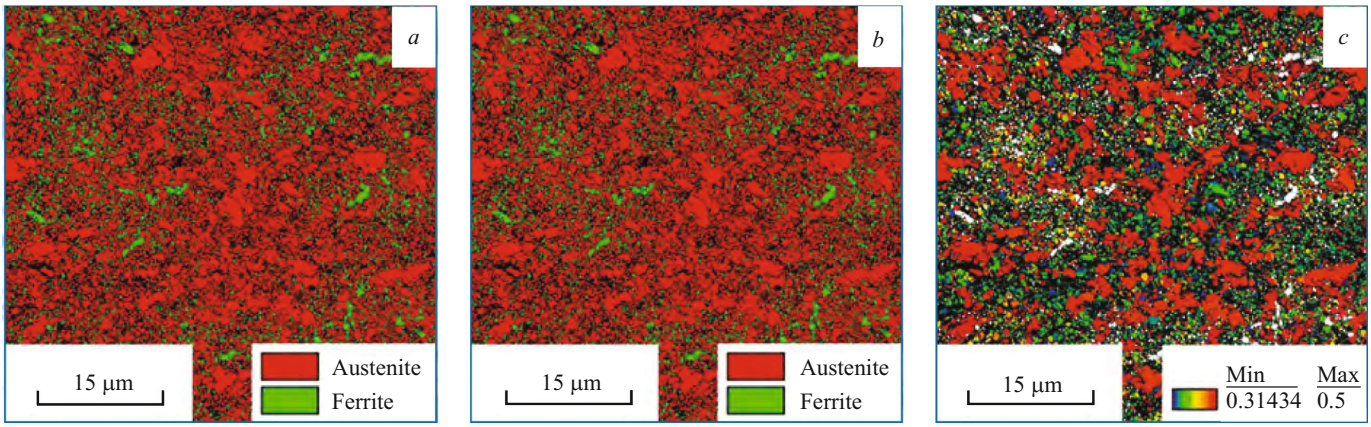


**Fig. 6.** Phase maps for the center (*a*) and for the surface layer (*b* ), and map of distribution of the Schmidt factor in the center (*c*) for twinning of austenite over the system of planes {111} and directions ⟨112⟩ of a bar from steel 08Kh18N10T after cold radial forging and annealing at 650°C.

Table 1). The coarsening of the structure is determined much by the decrease in the content of strain martensite (Fig. 1*a* ) and by the coagulation of carbides [15, 20]. The proportion of the grains with orientations $\langle 001\rangle_A \parallel$ PA and $\langle 111\rangle_A \parallel$ PA at the surface of the bar after annealing by all the tested variants remains invariable, i.e., 5 – 7 and 35% respectively (see Table 1).

***Mechanical properties after annealing at different temperatures.*** Right after the CRF to 90% and annealing at 400 and 500°C, the stress-strain curves do not have a region of uniform plastic strain, and the ductility is determined by the localized strain (Fig. 7*a* ). As compared to the state after the 90% CRF, the ultimate strength after the annealing at 400 and 500°C increases by 10%, and the elongation decreases inconsiderably, i.e., from 11.2 to 9.5% (Fig. 7*b* ). This effect should be associated chiefly with the precipitation hardening with nanocarbides of type $M_{23}C_6$ (Fig. 3*c* ). Elevation of annealing temperature to 550 – 700°C is accompanied by lowering of the strength characteristics (Fig. 7*b* ) due to formation of coarser carbides and simultaneous development of a reverse $\alpha \rightarrow \gamma$ transformation and recrystallization (Fig. 3). It should be noted that when the annealing temperature is raised within 400 – 700°C, the elongation increases gradually from 9.5 to 24% (Fig. 7*b* ). The dependence of the contraction on the annealing temperature exhibits a maximum at 650°C (Fig. 7*b* ). By the data of the EBSD analysis, the structure formed at this temperature consists of clusters of fine dispersed grains of martensite and austenite with orientations $\langle 111\rangle_A \parallel$ PA and $\langle 101\rangle_M \parallel$ PA and coarse austenite grains with orientation $\langle 001\rangle_A \parallel$ PA. Analysis of the Schmidt factor for twinning shows (Fig. 6*c* ) that this factor has high values (0.45 – 0.5) for coarse grains. However, the fine grains have a lower level of the Schmidt factor, which should cause appearance of reverse stresses and synergy of the strength and of the ductility [22].

When the annealing temperature is increased in the range of 700 – 900°C, the ultimate strength of the bar decreases substantially, while the ductility characteristics increase due to coagulation of the carbide phase and coarsening of the structure of the steel (see Table 1) as a result of recrystallization.

The dependence of the impact toughness (*KCT*) on the annealing temperature has two well manifested maximums at 500 and 650°C at the level of 1.25 – 1.42 MJ/m$^2$ (Fig. 7*b* ), which is close to the value of the *KCT* of the steel directly before the deformation [6]. The samples for the *KCT* tests have been cut over the axis of the bar. As a result, the crack propagated across all the layers of the gradient structure formed under the CRF and subsequent annealing.

Analyzing the fracture surfaces, we established that the fracture mechanism developed after the CRF by a microductile mechanism both in the center and in the surface layer

**TABLE 1.** Results of EBSD Analysis of the Steel Treated by Different Variants

| State | Proportion of grains, % | | Sharpness of inverse pole figure | | $D_{aust}$, μm |
|---|---|---|---|---|---|
| | ⟨111⟩ | ⟨001⟩ | ⟨111⟩ | ⟨001⟩ | |
| CRF + annealing at 650°C | 33/35 | 36/5 | 9.6/6.8 | 9.8/1.4 | 0.98 ± 0.01/0.63 ± 0.002 |
| CRF + annealing at 700°C | 23/35 | 42/7 | 5.4/6.7 | 12.5/1.4 | 1.8 ± 0.006/0.77 ± 0.002 |
| CRF + annealing at 800°C | 20/35 | 37/5 | 5.2/6.6 | 11.7/1.4 | 4.78 ± 0.014/3.94 ± 0.01 |

**Note.** The numerators present the results of the analysis of the orientation in the center of the sheet (over the thickness); the denominators give the same at the surface ($D_{aust}$ is the size of the austenite grains).

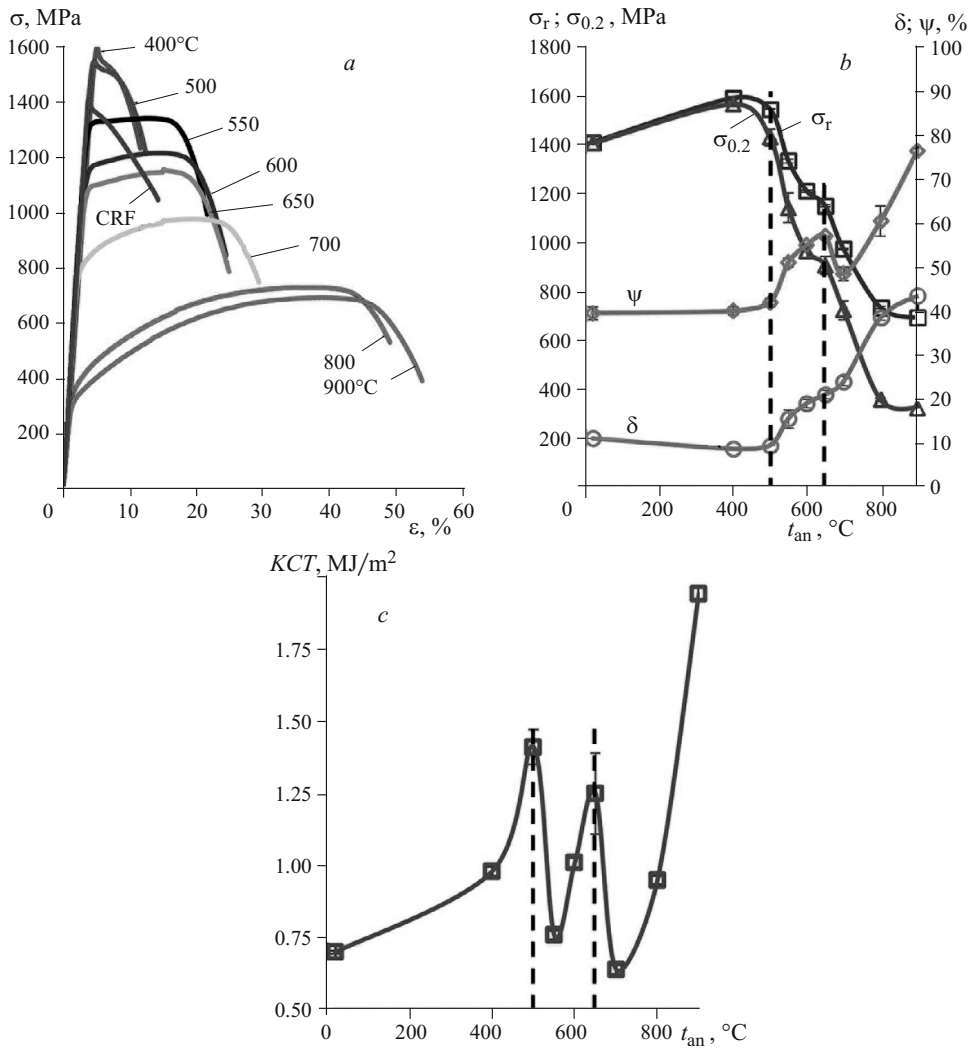


**Fig. 7.** Stress-strain diagrams (*a*) and dependences of mechanical properties on the annealing temperature in tensile tests (*b* ) and in impact bending tests (*c*).

(Fig. 8*a*, *d* and *g* ). After the annealing at 500°C, the center of the bar fractured by a microductile mechanism and the surface layer fractured along and across the fibers (Fig. 8*b*, *e* and *h* ), i.e., stepwise. This seems to be caused by suppression of the formation of pores by nanocarbides and by partial weakening of the boundaries of the fiber structure formed under the CRF (Fig. 2*d* ) due to precipitation of nanocarbides on them [14].

The high impact toughness of the steel after the annealing at 650°C (Fig. 7*b* ) is a result of formation of a structure represented by clusters of fine dispersed austenite and martensite grains with orientations $\langle 111\rangle_A \parallel$ PA and $\langle 101\rangle_M \parallel$ PA and coarse austenite grains with orientation $\langle 001\rangle_A \parallel$ PA, because the gradient of the phase composition and of the hardness in this case is weak. After the tests, a microductile (dimple) fracture is present simultaneously in the center and in the surface layer of the sample (Fig. 8*c*, *f* and *i* ). Such annealing is characterized by maximum contraction (Fig. 7*b* ). It should be noted that we conducted uniaxial tension of samples cut from the core of the bar, i.e., the peak of the contraction indicated enhanced toughness of the core. Since the contraction of homogeneous materials depends directly on the impact toughness [23], it seems natural that the contraction maximum coincides with the maximum of the impact toughness.

Thus, the two most interesting structures have been obtained as a result of the post-deformation at 500 and 650°C. Cold radial forging of degree 90% produces a pronounced gradient of phase composition over cross section, and it is preserved after the annealing at 500°C (Fig. 1*a* ). In addition, $M_{23}C_6$-type nanocarbides precipitate inside and over the boundaries in the regions of strain martensite (Fig. 3*b* ), which is accompanied by growth of the hardness (Fig. 1*b* ) firstly in the surface layers, where the micromechanism of fracture changes in the tests for impact toughness (Fig. 8*e* and *h* ). In addition to the considerable hardening (Fig. 7*b* ), this effect causes considerable increase of the impact toughness *KCT* (Fig. 7*c* ).

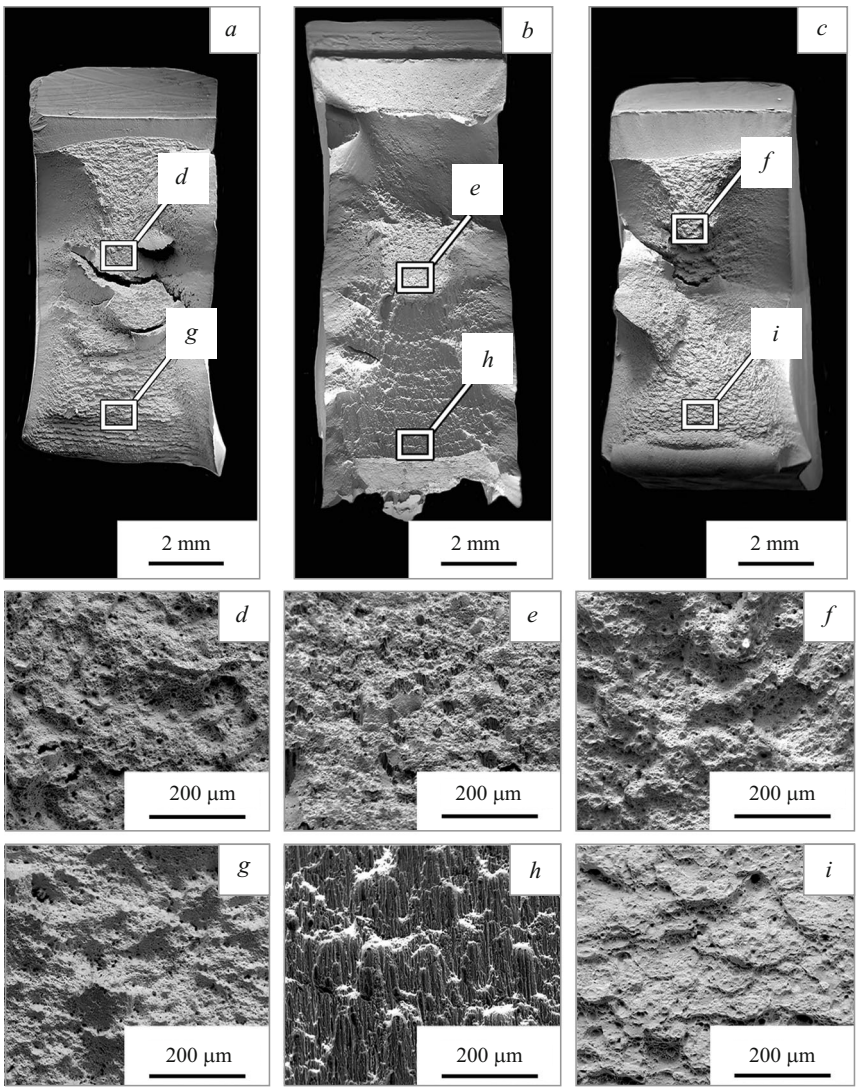


**Fig. 8.** Fractures of specimens of the steel treated by different variants after testing for impact bending (*KCT*): *a*, *d*, *g*) after CRF; *b*, *f*, *h*) after CRF and annealing at 500°C; *c*, *f*, *i*) after CRF and annealing at 650°C; *a* – *c*) general view; *d* – *i*) magnified enframed structures.

After the annealing at 650°C, the center of the bar acquires a structure represented by clusters of fine austenite and martensite grains and coarse austenite grains (Fig. 5*a*). This is connected with the nonuniform distribution of strain martensite grains that retard the growth of austenite grains. The regions containing clusters of martensite grains preserve a fine-grained structure and vice versa (Fig. 6*a*). Moreover, the coarse austenite grains are oriented $\langle 001\rangle_A \parallel$ PA and the fine grains of austenite and martensite have orientations $\langle 111\rangle_A \parallel$ PA and $\langle 101\rangle_M \parallel$ PA respectively (Fig. 5*a*). This structural state provides a high level of impact toughness (Fig. 7*a*) and ductility in combination with elevated strength characteristics (Fig. 7*b*).

## CONCLUSIONS

We have studied the effect of heat treatment (annealing at different temperatures) on the evolution of gradient structure in metastable austenitic stainless steel 08Kh18N10T (type AISI 321) subjected to cold radial forging. The results of the study allow us to make the following conclusions.

1. Cold radial forging produces a phase composition gradient over the section of the bar containing about 40% α′-martensite in the surface layer and about 70% in the center. Subsequent low-temperature annealing at 500°C is accompanied by precipitation hardening due to precipitation of $M_{23}C_6$-type carbides mostly in the regions of strain α′-martensite.

2. Annealing at 500°C causes simultaneous considerable hardening ($\sigma_r > 1500$ MPa) and growth in the impact toughness ($KCT > 1.4$ MJ/m$^2$). The tests for impact toughness change the micromechanism of fracture in crack propagation from the center to the surface of the bar. For example, the center fractures by a microductile mechanism and the crack at the surface develops along and across the fibers, i.e., stepwise.

3. Post-deformation annealing at 650°C causes formation of a structure consisting of coarse austenite grains with ori-

entation $\langle 001 \rangle_A \parallel$ PA (parallel to the bar axis: $\parallel$ PA) and clusters of fine austenite and martensite grains with dominant orientations $\langle 111 \rangle_A \parallel$ PA and $\langle 101 \rangle_M \parallel$ PA, respectively, in the center of the bar. However, the structure at the surface of the bar is homogeneous and consists of only fine austenite and martensite grains with dominant orientations $\langle 111 \rangle_A \parallel$ PA and $\langle 101 \rangle_M \parallel$ PA, respectively. This structural state provides a favorable combination of strength ($\sigma_r > 1100$ MPa), ductility ($\delta > 20\%$) and impact toughness ($KCT \sim 1.3$ MJ/m$^2$ ).

*The work has been performed with financial support of the RSF (Grant No. 20-79-10094).*

## REFERENCES


1. J. Beddoes and J. G. Parr, *Introduction to Stainless Steels*, ASM International, Materials Park, OH, USA (1999), 315 p.
2. K. H. Lo, C. H. Shek, and J. K. L. Lai, "Recent developments in stainless steels," *Mater. Sci. Eng. R Rpt*., **65**(4 – 6), 39 – 104 (2009).
3. I. Shakhova, et al., "Effect of large strain cold rolling and subsequent annealing on microstructure and mechanical properties of an austenitic stainless steel," *Mater. Sci. Eng. A*, **545**, 176 – 186 (2012).
4. H. Ueno, et al., "Enhanced fatigue properties of nanostructured austenitic SUS 316L stainless steel," *Acta Mater.*, **59**(18), 7060 – 7069 (2011).
5. L. Üçok, T. Ando, and N. J. Grant, "Property enhancement in Type 316L stainless steel by spray forming," *Mater. Sci. Eng. A*, **133**(C), 284 – 287 (1991).
6. D. Panov, et al., "Metastable austenitic steel structure and mechanical properties evolution in the process of cold radial forging," *Materials (Basel)*, **12**(2058) (2019).
7. T. H. Fang, et al., "Revealing extraordinary intrinsic tensile plasticity in gradient nano-grained copper," *Science*, **331**(6024), 1587 – 1590 (2011).
8. X. L. Wu, et al., "Combining gradient structure and TRIP effect to produce austenite stainless steel with high strength and ductility," *Acta Mater.*, **112**, 337 – 346 (2016).
9. J. Gu, et al., "Effects of grain size on the microstructures and mechanical properties of 304 austenitic steel processed by torsional deformation," *Micron*, **105**, 93 – 97 (2018).
10. H. W. Huang, et al., "Fatigue behaviors of AISI 316L stainless steel with a gradient nanostructured surface layer," *Acta Mater.*, **87**, 150 – 160 (2015).
11. Y. B. Lei at al., "Enhanced mechanical properties and corrosion resistance of 316L stainless steel by pre-forming a gradient nanostructured surface layer and annealing," *Acta Mater.*, **208** (2021).
12. Z. Zeng, et al., "Gradient plasticity in gradient nano-grained metals," *Extrem. Mech. Lett. Elsevier Ltd*, **8**, 213 – 219 (2016).
13. D. O. Panov, et al., "Excellent strength-toughness synergy in metastable austenitic stainless steel due to gradient structure formation," *Mater. Lett*., **303**, July, 130585 (2021).
14. D. Panov, et al., "Effect of cold swaging on the bulk gradient structure formation and mechanical properties of a 316-type austenitic steel," *Materials (Basel)*, **15**(7), 2468 (2022).
15. D. Panov, et al., "Mechanisms of the reverse martensite-to-austenite transformation in a metastable austenitic stainless steel," *Metals (Basel)*, **11**(4), 1 – 13 (2021).
16. A. Weidner, U. D. Hangen, and H. Biermann, "Nanoindentation measurements on deformation-induced α-martensite in a metastable austenitic high-alloy CrMnNi steel," *Philos. Mag. Lett*., **94**(8), 522 – 530 (2014).
17. G. Singh, et al., "Finite element analysis and experimental evaluation of residual stress of Zr-4 alloys processed through swaging," *Metals (Basel)*, **10**(10), 1 – 15 (2020).
18. H. Wen, et al., "Strengthening mechanisms in a high-strength bulk nanostructured Cu – Zn – Al alloy processed via cryomilling and spark plasma sintering," *Acta Mater.*, **61**(8), 2769 – 2782 (2013).
19. D. O. Panov, et al., "Excellent strength-toughness synergy in metastable austenitic stainless steel due to gradient structure formation," *Mater. Lett*., **303**, July, 130585 (2021).
20. A. Aletdinov, et al., "Martensite-to-austenite reversion and recrystallization in cryogenically-rolled type 321 metastable austenitic steel," *Metall. Mater. Trans. A, Phys. Metall. Mater. Sci*., **50**(3), 1346 – 1357 (2019).
21. D. Panov, et al., "Gradient microstructure and texture formation in a metastable austenitic stainless steel during cold rotary swaging," *Materials (Basel)*, **16**(4), 1 – 16 (2023).
22. X. Wu and Y. Zhu, "Heterogeneous materials: a new class of materials with unprecedented mechanical properties," *Mater. Res. Lett*., **5**(8), 527 – 532 (2017).
23. V. A. Bubnov and S. G. Kostenko, "Mechanism of hardening of austenitic steels under plastic deformation," *Izv. Vysh. Uchebn. Zaved., Mashinostr.*, **6**, 63 – 70 (2008).